Journal of Applied Fluid Mechanics, Vol. 12, No. 2, pp. 573-586, 2019.
Available online at www.jafmonline.net, ISSN 1735-3645, EISSN 1735-3645.
DOI: 10.29252/jafm.12.02.28618

Performance Evaluation of Insoluble Surfactants on the Behavior of Two Electric Layers

S. A. Alkharashi[1,2†], A. Assaf[3], K. Al-Hamad[1] and A. Alrashidi[1]

[1] *Applied Sciences Department, College of Technological Studies, PAAET, Kuwait*
[2] *Quesna Technical College, Ministry of Higher Education, Cairo, Egypt*
[3] *Mathematics Department, Faculty of Science, Helwan University, Egypt*

†*Corresponding Author Email: sa.alkharashi@paaet.edu.kw*

(Received November 25, 2017; accepted September 5, 2018)

ABSTRACT

The purpose of this study is to establish the effects of insoluble surfactants on the stability of two layers flow down an inclined wall in the limit of Stokes and long-wavelength approximations. The dynamics of the liquid-liquid interface is described for arbitrary amplitudes by evolution equations derived from the basic hydrodynamic equations, in which the fluids are subjected to a uniform electric field. The principle aim of this work is to investigate the interfacial stability as well as the growth rate in the presence of insoluble surfactants. The parameters governing the flow system, such as Marangoni, Weber, capillary numbers and the inclined substrate strongly affect the waveforms and their amplitudes and hence the stability of the fluid. Approximate solutions of this system of linear evolution equations are performed. epending on the selected parameters, the phenomenon of the dual role is found with respect to the electric Weber number as well as the viscosity ratio. The interfacial waves will be more stable due to the growth of the Marangoni number while, while the opposite effect is found for the increase in capillary number. In the longwave perturbations, the stability process is found to confirm the stabilizing effect of the Marangoni number and the destabilizing influence of both capillary and Reynolds numbers, whereas the dual role is observed for the dielectric ratio.

Keywords: Insoluble surfactants; Inclined substrate; Viscous fluids; Electric field; Long wave analysis.

1. INTRODUCTION

The presence of surfactants in multiphase systems has a significant influence on the shape and the motion of the interfaces. Surfactants also have a wide range of applications in the oil industry, for example in the cleanup of oil spills and the enhancement of oil recovery. This has motivated the increasing interest to understand the effect of surfactants on the interfacial behavior in recent years. A large number of investigations has been devoted to the insoluble surfactant limit. In particular, in the limit of vanishing Reynolds number Pozrikidis (2003), has investigated the effect of an insoluble surfactant on the gravity-driven flow of a liquid film down an inclined wall with periodic undulations or indentations. When the film thickness is less than half the wall period it is found that the surfactant is most significant .

The approach proposed by Gao and Lu (2007), is limited to study the effect of insoluble surface and interfacial surfactants on the inertialess instability of a two-fluid film flow down an inclined plane. The results reveal that the inertialess instability of relatively long waves can be predominantly weakened by a surface surfactant and enhanced by an interfacial surfactant. Luo and Pozrikidis (2007), have analyzed the gravity-driven flow of a liquid film down an inclined wall with three-dimensional doubly periodic corrugations in the limit of vanishing Reynolds number, where the film surface may exhibit constant or variable surface tension due to an insoluble surfactant.

The stability of a liquid film flowing down an inclined plane when the film is contaminated by an insoluble surfactant and subjected to a uniform normal electric field is investigated in the work by Blyth (2008). The stability characteristics of Stokes flow are described exactly and the growth rates of the normal modes at finite Reynolds number are computed numerically. The long-wave Marangoni convection in a horizontal liquid layer with insoluble surfactant absorbed on the free surface is studied by Mikishev and Nepomnyashchy (2010). They considered that the surfactant is convected by interfacial velocity field and located over the interface but not into the bulk of the fluid.

Yiantsios and Higgins (2010), have examined the mechanism of Marangoni instability in evaporating thin liquid films due to soluble surfactant. A thin-film analysis is applied and evolution equations for the film thickness and the surfactant concentration are derived and analyzed by the techniques of linear stability and numerical simulation. Sirwah (2012), has discussed the linear stability analysis of the electrified surface separating two coaxial Oldroyd-B fluid layers confined between two impermeable rigid cylinders in the presence of both interfacial insoluble surfactant and surface charge through porous media. The author referred that the influence of the physicochemical parameter is to decrease the instability region of the surface and reduce the growth rate of the unstable normal modes.

Uma and Usha (2012), have investigated the two-dimensional flow of a thin layer of a viscous perfectly conducting liquid film down an inclined plane in the presence of a uniform electric field at infinity and, perpendicular to the unperturbed interface, when an insoluble surfactant is diffused at the interface. Park *et al*. (2013), have analyzed the effect of insoluble surfactant on drop formation in a capillary microfluidic device. They used a diffuse-interface method to describe the evolution of interface involving insoluble surfactant and solved the Navier-Stokes/Cahn-Hilliard equations and the surfactant conservation equation by the finite element method with a grid deformation method. A lot of works are devoted to the Marangoni convection through the interfacial insoluble surfactants can be found in the papers Halpern and Frenkel (2003), Blyth and Pozrikidis (2004), Mikishev and Nepomnyashchy (2011), André and Bardet (2015); Allias *et al*. (2017).

The focus of this work is to survey and develop a mathematical model for two falling films confined between two rigid plates in the presence of interfacial insoluble surfactants. An analytical and numerical solutions to the considered problem are obtained, in which the fluids are subjected to an electric field normal to the flow direction. The aim here is to study the effect of the surfactants on the stability of the fluids flow under the effect of the electric field. The present article is structured as follows. This section has presented the motivation for the investigation in addition to relevant background information. The next section lays down the theoretical preliminaries and basic equations. The third section provides a description of the Stokes flow, in which the characteristic equation that controls the stability configuration has been derived. Also in this section numerical estimations for the effect of various problem-properties on the stability of the interface have been discussed, where some stability diagrams are plotted and studied. In the fifth section, the case of long wave interfacial stability has been investigated. The results are discussed and some important conclusions are drawn in the final section of this paper.

2. THEORETICAL PRELIMINARIES AND BASIC EQUATIONS

2.1 Description

The physical model of a two-dimensional flow is illustrated in Fig. 1. Two bounded viscous liquid layers of constant density $\rho^{(r)}$ and viscosity $\mu^{(r)}$, flows under gravity along an infinitely long flat plate which is inclined at an angle β to the horizontal. The superscript r = 1, 2 represents lower layer (fluid 1) and the upper layer (fluid 2). A Cartesian coordinate system (x,y) is adopted such that x−axis measuring distance down along the flow in which the fluids are assumed to be unbounded in x−direction and y−axis being measured perpendicular to it.

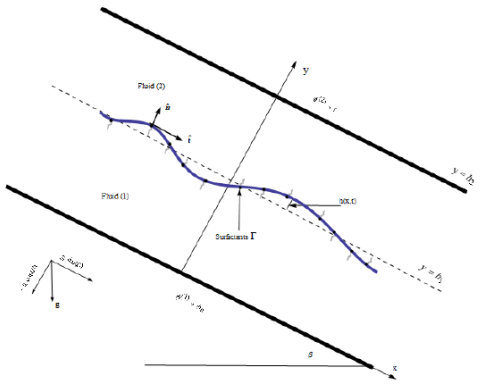

Fig. 1. Schematic of the problem.

It is assumed that the two fluids are thus subjected to normal electric field $E^{(r)}$, in which the lower plate (y = 0) is energized at the constant electric potential φ0, while the upper one ($y = h_2$) is grounded so that its electric potential is zero. The lower-film thickness is $h_1 + h(x,t)$ while the upper-film thickness is $h_1 - h(x,t)$ since h is the height of the disturbed interface measured from the unperturbed level $y = h_1$. In the inclined system of coordinates employed here, the components of the acceleration due to gravity g are $g_x = g\sin\beta$ and $g_y = -g\cos\beta$. Surfactants with surface concentration $\Gamma(x,t)$ are localized on the interface separating the two fluids. Its distribution is dependent on time and the concentration of the insoluble surfactants is governed, by the following expression (Mikishev and A. A. Nepomnyashchy (2010), Yiantsios and Higgins (2010), Sirwah (2012), Uma and R. Usha (2012); Park *et al*. (2013)).

$$\frac{\partial \Gamma}{\partial t} + \nabla_s \cdot \left(\Gamma \mathbf{u}_s\right) = -\Gamma \kappa u_n + D_s \nabla_s^2 \Gamma. \tag{1}$$

In this equation u_s is the tangential velocity, u_n denotes interfacial velocity in the direction of the normal vector. The symbol ∇_s denotes the surface gradient, κ refers to local surface curvature and D_s is the surface diffusivity. For the flat nondeformable interface, the above equation can be written as

$$\frac{\partial \Gamma}{\partial t}+\frac{\partial\left(u_t \Gamma\right)}{\partial l}=D_s \frac{\partial^2 \Gamma}{\partial l^2}, \tag{2}$$

where, u_t refers to the tangential velocity at the interface and l is the arc length increasing in the direction of the unit tangent vector. Since we are concerned with small deformation theory for the linear stability problem, the interfacial tension γ is a function of surfactant concentration Γ and the relation between them can be approximated, using Taylor series expansion around the reference value Γ_0, as

$$\gamma=\gamma_0-E\left(\Gamma-\Gamma_0\right), \tag{3}$$

where $E=-\left(\partial \gamma / \partial \Gamma\right)_{\Gamma_0}$ is the surfactant elasticity, and Γ_0 is the basic value of the surfactant concentration, corresponding to the uniform interfacial tension γ_0.

2.2 Transport Equations in Bulk Phases

The hydrodynamics relation governing the fluid velocities and the pressure in the bulk of the two viscous layers can be rendered in the following dimensional equation

$$\rho^{(r)} \frac{d \mathbf{V}^{(r)}}{d t}=-\nabla p^{(r)}+\mu^{(r)} \nabla^2 \mathbf{V}^{(r)}+\rho^{(r)} \mathbf{g}. \tag{4}$$

For incompressible fluid flow, the associated continuity equation is a mathematical statement that, in any steady state process, the rate at which mass enters a system is equal to the rate at which mass leaves the system and is based on the principle of conservation of mass, which reads

$$\nabla \cdot \mathbf{V}^{(r)}=0 \tag{5}$$

Here $d / d t \equiv \partial / \partial t+\left(\mathbf{V}^{(r)} \cdot \nabla\right)$ stands for the convective derivative, $\mathbf{V}=\left(U(y)+u, v\right)$ represents the total velocity vector in the fluid films and $\nabla \equiv\left(\partial / \partial x, \partial / \partial y\right)$ is the horizontal gradient operator.

In formulating Maxwell's equations for the problem, we supposed that the electro-quasi-static approximation is valid for the problem, i.e. the effects of the magnetic fields due to the slow variations in the electric fields are negligible. This assumption requires that the electric field and the displacement vector assume zero curl and divergence respectively and consequently we have

$$\nabla .\left(\varepsilon^{(r)} \mathbf{E}^{(r)}\right)=0 \text{ and } \nabla \times \mathbf{E}^{(r)}=\mathbf{0}. \tag{6}$$

Here, $\mathbf{E}^{(r)}$ is the electric field intensity vector, the notation × refers to the vector product of two vectors and $\varepsilon^{(r)}$ refers to the dielectric constant. The construction of a potential function $\phi^{(r)}$, can be given as the gradient of the scalar potential such that

$$\mathbf{E}^{(r)}=E_0^{(r)} \hat{\mathrm{y}}-\nabla \phi^{(r)}, \tag{7}$$

where, $\hat{\mathrm{y}}$ is a unit vector along y−direction. This equation automatically satisfies zero curl for a constant permittivity and therefore the electrostatic potential satisfies the Laplace equation

$$\nabla^2 \phi^{(r)}=0. \tag{8}$$

2.3 Boundary Conditions

Here, the boundary constraints are information about the obtained solutions of the governing equations at certain places, such as the lower and the upper substrates, in addition the interface between the fluids (Shankar and Sharma (2004), Wu and Chou (2005), Ozen *et al*. (2006), Zakaria *et al*.(2009), Hayat *et al*. (2016), Alkharashi and Gamiel (2017), Tomar *et al*. (2007); Zakaria and Alkharashi (2017)).

At the interface $y=h_1 \pm h(x, t)$, it is natural to impose the kinematic boundary condition which is essentially geometrical, and a physical condition of force balance. When there is no cavitation in the interface between the fluids, the kinematic condition in which the interface always comprises the same fluid particles is imposed, and therefore the function $h(x,t)$ whose graph defines the interface satisfies simultaneously

$$\frac{d y}{d t}=\left(\frac{\partial}{\partial t}+\mathbf{V}^{(r)} \cdot \nabla\right) h(x, t). \tag{9}$$

The normal component of the velocity vector in each of the phases of the system is continuous at the dividing surface:

$$\hat{\mathbf{n}} \cdot\left(\mathbf{V}^{(1)}-\mathbf{V}^{(2)}\right)=0. \tag{10}$$

No-slip condition at the interface between the layers (the tangential component of the velocity vector is continuous):

$$\hat{\mathbf{t}} \cdot\left(\mathbf{V}^{(1)}-\mathbf{V}^{(2)}\right)=0. \tag{11}$$

where $\hat{\boldsymbol{n}}=\nabla F /|\nabla F| \approx(-\partial h / \partial x, 1)$ is the exterior pointing normal unit vector to the interface, $\hat{\mathbf{t}} \approx(1,-\partial h / \partial x)$ is the corresponding unit tangent and $F=y-\left(h_1-h(x, t)\right)=0$ is the surface geometry.

The boundary conditions on the upper and lower plates, in which the plates are assumed to be rigid and kept constants, imply that all velocity components have to be zero there (since the fluids adhere to the plates):

$$\mathbf{V}^{(1)}=0 \text{ at } y=0 \text{ and } \mathbf{V}^{(2)}=0 \text{ at } y=h_2. \tag{12}$$

Using Maxwell's conditions on the electric field where no free surface charges are present on the interfaces, the continuity of the normal component of the electric displacement at the interface gives:

$$\hat{\mathbf{n}}\cdot\left(\varepsilon^{(1)}\mathbf{E}^{(1)}-\varepsilon^{(2)}\mathbf{E}^{(2)}\right)=0. \tag{13}$$

In addition, since the fluids are assumed perfect conductor, the continuity of the tangential component of the electric field across the interface implies that

$$\hat{\mathbf{t}}\cdot\left(\mathbf{E}^{(1)}-\mathbf{E}^{(2)}\right)=0. \tag{14}$$

Beside the continuity of the tangential and normal velocity as well as the electric field and flux density, there are two important sets of conditions determine the behavior of the stress tensor at the surface between the two fluids:

The normal stresses are balanced by the amount of the surface tension (the dynamical boundary condition):

$$\hat{\mathbf{n}}\cdot\left\|-p\mathbf{I}+\tau\right\|\cdot\hat{\mathbf{n}}=-\gamma(\Gamma)\nabla\cdot\hat{\mathbf{n}}. \tag{15}$$

The stress tensor, τ, is composed of the deviatoric viscous stresses for the Newtonian fluid, τ_{vis}, and an electrical component which describes the stress field induced in the material due to electrostatic forces, τ_{elec}. The expressions of these stresses follow the relations

$$\tau_{vis}^{(r)}=\mu^{(r)}\left(\nabla\mathbf{V}^{(r)}+\nabla\mathbf{V}^{(r)^T}\right), \tag{16}$$

$$\tau_{elec}^{(r)}=\varepsilon^{(r)}\left(\mathbf{E}^{(r)}\mathbf{E}^{(r)}-\frac{1}{2}\left(\mathbf{E}^{(r)}\cdot\mathbf{E}^{(r)}\right)\mathbf{I}\right). \tag{17}$$

Here, in these equations the symbol I denotes the identity tensor, the superscript T indicates the matrix transpose, while the notation || || denotes a jump in any scalar or vector quantity as the interface is crossed from the lower layer to the upper one. The second condition is the equilibrium of the tangential stress tensor across the interface, which requires

$$\hat{\mathbf{n}}\cdot\left\|\tau\right\|\cdot\hat{\mathbf{t}}=\nabla\gamma(\Gamma)\cdot\hat{\mathbf{t}}. \tag{18}$$

In this condition, is to be noted that the electric field through Maxwell stresses does not contribute to the tangential stress balance at the interface, which includes only the effect of the surfactant since we deal with a perfect conductor model. This can be deduced directly for the present work by substituting condition (14) into (18), where the term corresponding to the electric field in the tangential stress tensor is the same of condition (14), and hence can be neglected.

3. DIMENSIONLESS EQUATIONS AND SOLUTIONS

In writing the governing equations, the boundary conditions and also solutions of the considered problem in the dimensionless arguments, the dimensionless process is chosen such that the distance between the two plates h_2 represents as the length scale and the characteristic velocity scale is defined by $U_c=\rho^{(1)}gh_2^2\sin\beta/\mu^{(1)}$. The time and the pressure have dimensionless h_2/U_c and $\mu^{(1)}U_c/h_2$ respectively. Also the surfactants and the electric potential are removed from dimension using Γ_0 and E_0h_2. After using these scales to nondimensionalize the above governing equations and boundary conditions, we have the following nondimensional set of equations:

$$\hat{\rho}^{(r)}R_e\frac{d\mathbf{V}^{(r)}}{dt}=-\nabla p^{(r)}+\hat{\mu}^{(r)}\nabla^2\mathbf{V}^{(r)}+\hat{\rho}^{(r)}(1,-\cot\beta), \tag{19}$$

where, $\hat{\rho}^{(r)}=\rho^{(r)}/\rho^{(1)}$ represents the fluid density ratio appears in fluid 2, the parameter $\hat{\mu}^{(r)}=\mu^{(r)}/\mu^{(1)}$ is the ratio of the dynamic viscosities appears in the upper fluid, $R_e=\rho^{(1)}h_2U_c/\mu^{(1)}$ denotes the Reynolds number of the lower-layer flow, which measures the relative strength between the inertial and viscous forces. The continuity equation and the electric potential relation still unchange due to the dimensionless process which read

$$\frac{\partial u^{(r)}}{\partial x}+\frac{\partial v^{(r)}}{\partial y}=0, \tag{20}$$

$$\frac{\partial^2\phi^{(r)}}{\partial x^2}+\frac{\partial^2\phi^{(r)}}{\partial y^2}=0. \tag{21}$$

In order to obtain the linear stability approach for the pervious system of governing equations and the corresponding boundary conditions. The system will be affected by small two-dimensional perturbations. Let us label the basic state quantity by the subscribe *b* a perturbation one is denoted by have the subscribe *p*. Now, to get the main-flow solutions of the velocity and the electric potential, we use the zero order of the governing equations and the corresponding boundary conditions. Hence the solutions of the basic pressure $p_0^{(r)}$, velocity $U^{(r)}$ and the potential $\phi_b^{(r)}$ are given by

$$\begin{aligned} p_0^{(r)}&=-\hat{\rho}^{(r)}\cot\beta y+\hat{p}_0,\\ U^{(r)}(y)&=-\frac{\hat{\rho}^{(r)}}{2\hat{\mu}^{(r)}}y^2+a_1^{(r)}y+a_2^{(r)},r=1,2, \end{aligned} \tag{22}$$

$$\begin{aligned} \phi_b^{(1)}(y)&=\left\{1-\frac{\hat{\varepsilon}y}{1+(\hat{\varepsilon}-1)h_0}\right\}\phi_0,\\ \phi_b^{(2)}(y)&=\frac{(1-y)\phi_0}{1+(\hat{\varepsilon}-1)h_0}, \end{aligned} \tag{23}$$

where $\hat{p}_0$ refers to the constant of integration and h_0 is the ratio h_1/h_2,

$$a_1^{(1)} = \frac{h_0\left\{2+h_0\left(\hat{\mu}^{(2)}-2\right)\right\}\hat{\rho}^{(2)}\left(h_0-1\right)^2}{2\left\{1+h_0\left(\hat{\mu}^{(2)}-1\right)\right\}},\quad a_2^{(1)}=0,$$

$$a_1^{(2)} = \frac{\hat{\rho}^{(2)}\left\{1+h_0^2\left(2\hat{\mu}^{(2)}-1\right)\right\}-h_0^2\hat{\mu}^{(2)}}{2\left\{1+h_0\left(\hat{\mu}^{(2)}-1\right)\right\}},$$

$$a_2^{(2)} = \frac{h_0^2\hat{\rho}^{(2)}+h_0\hat{\rho}^{(2)}\left\{\hat{\mu}^{(2)}\left(1-2h_0\right)+h_0-1\right\}}{2\left\{1+h_0\left(\hat{\mu}^{(2)}-1\right)\right\}}.$$

Consider the normal mode expansions to express the solution as

$$\left\{h(x,t),\Gamma(x,t)\right\}=\left\{\hat{h},\hat{\Gamma}\right\}e^{ik(x-ct)}+c.c, \tag{24}$$

where $\hat{h}$ and $\hat{\Gamma}$ are disturbance amplitudes of the applied perturbation, k is the real and positive wave number, $c = c_r + ic_i$ is a complex eigenvalue with c_r as the wave speed, and c_ik is the growth rate. The state, $c_i > 0$ introduces an unstable mode, while the converse expects a stable one and when c_i vanishes the system is neutrally stable. The symbol *c.c* denotes the complex conjugate for the previous complex terms.

In accordance with the interface deflections given by (24) and in view of a standard Fourier decomposition, we may similarly assume that the solution of the perturbed quantities is functions of both the horizontal and vertical coordinates as well as the time:

$$F(x,y,t)=\hat{F}(y)e^{ik(x-ct)}+c.c. \tag{25}$$

The solution of the above system of governing equations and boundary conditions can be facilitated by defining a stream function, $\psi^{(r)}(x,y,t)$, which automatically satisfies Eq. (20) and is related to the velocity perturbations so that $u^{(r)} = \partial\psi^{(r)}/\partial y$ and $v^{(r)} = -\partial\psi^{(r)}/\partial x$. Eliminating the pressure term, by applying the curl operator on Eq. (19), then using (25), we derive the Orr-Sommerfeld equations

$$\frac{d^4\hat{\psi}^{(r)}}{dy^4}-2k^2\frac{d^2\hat{\psi}^{(r)}}{dy^2}+k^4\hat{\psi}^{(r)}=ik\frac{\hat{\rho}^{(r)}}{\hat{\mu}^{(r)}}R_e\left\{\left(U^{(r)}-c\right)\left(\frac{d^2\hat{\psi}^{(r)}}{dy^2}-k^2\hat{\psi}^{(r)}\right)-\frac{d^2U^{(r)}}{dy^2}\hat{\psi}^{(r)}\right\}, \tag{26}$$

for r = 1,2. To satisfy the no-slip and impermeability conditions at the rigid walls, we require that

$$\hat{\psi}^{(1)}=\frac{d\hat{\psi}^{(1)}}{dy}=0 \quad \text{at} \quad y=0,$$

$$\hat{\psi}^{(2)}=\frac{d\hat{\psi}^{(2)}}{dy}=0 \quad \text{at} \quad y=1. \tag{27}$$

The linearized versions of the boundary conditions at the interface can be obtained by applying Taylor expansion on the exact conditions in powers of h around their main positions and then retaining the leading-order terms. Taking the linear terms of the dimensionless form of the normal stress balance Eq. (15) at the dividing surface yields:

$$\begin{aligned}&\frac{\partial^3\boldsymbol{\psi}^{(1)}}{\partial y^3}-\hat{\mu}^{(2)}\frac{\partial^3\boldsymbol{\psi}^{(2)}}{\partial y^3}+3\left\{\frac{\partial^3\boldsymbol{\psi}^{(1)}}{\partial x^2\partial y}+\hat{\mu}^{(2)}\frac{\partial^3\boldsymbol{\psi}^{(2)}}{\partial x^2\partial y}\right\}\\&-R_e\left\{U^{(1)}\frac{\partial^2\boldsymbol{\psi}^{(1)}}{\partial x\partial y}-\hat{\rho}^{(2)}U^{(2)}\frac{\partial^2\boldsymbol{\psi}^{(2)}}{\partial x\partial y}\right\}-R_e\left\{\frac{\partial^2\boldsymbol{\psi}^{(1)}}{\partial y\partial t}\right.\\&\left.-\hat{\rho}^{(2)}\frac{\partial^2\boldsymbol{\psi}^{(2)}}{\partial y\partial t}\right\}+R_e\left\{\frac{\partial U^{(1)}}{\partial y}\frac{\partial\boldsymbol{\psi}^{(1)}}{\partial x}-\hat{\rho}^{(2)}\frac{\partial U^{(2)}}{\partial y}\right.\\&\left.\times\frac{\partial\boldsymbol{\psi}^{(2)}}{\partial x}\right\}-W_e\left\{\frac{\partial\hat{\phi}^{(1)}}{\partial y}\frac{\partial^2\tilde{\phi}^{(1)}}{\partial x\partial y}-\hat{\varepsilon}\frac{\partial\hat{\phi}^{(2)}}{\partial y}\frac{\partial^2\tilde{\phi}^{(2)}}{\partial x\partial y}\right\}\\&+\left(1-\hat{\rho}^{(2)}\right)\cot\beta\frac{\partial h}{\partial x}+2\left\{\frac{\partial U^{(1)}}{\partial y}-\hat{\mu}^{(2)}\frac{\partial U^{(2)}}{\partial y}\right\}\frac{\partial^2 h}{\partial x^2}\\&+\frac{1}{C_a}\frac{\partial^3 h}{\partial x^3}=0.\end{aligned} \tag{28}$$

The condition for the jump in the tangential stress component at the interface is obtained by neglecting the quadratic terms in of Eq. (18) and using the linearized dimensionless forms of the relations (2) and (3), one gets

$$\begin{aligned}&\frac{\partial^2\boldsymbol{\psi}^{(1)}}{\partial y^2}-\frac{\partial^2\boldsymbol{\psi}^{(1)}}{\partial x^2}-\hat{\mu}^{(2)}\left\{\frac{\partial^2\boldsymbol{\psi}^{(2)}}{\partial y^2}-\frac{\partial^2\boldsymbol{\psi}^{(2)}}{\partial x^2}\right\}\\&+\frac{M_a}{C_a}\frac{\partial\Gamma}{\partial x}=0.\end{aligned} \tag{29}$$

The linearized dimensionless form of the surfactant transport Eq. (2) in the general case of unsteady flow is

$$\frac{\partial\Gamma}{\partial t}+U^{(1)}\frac{\partial\Gamma}{\partial x}+\frac{\partial U^{(1)}}{\partial y}\frac{\partial h}{\partial x}+\frac{\partial^2\boldsymbol{\psi}^{(1)}}{\partial x\partial y}=0, \tag{30}$$

where all terms are evaluated at $y = h_1$. Here, in deriving this equation the term in the right hand side of Eq. (2) is ignored, where in most practical applications, the surfactant diffusivity is very small such that it can be canceled. In addition the third term on the left hand side in Eq. (30) arises from the derivative

$$\partial U^{(1)}/\partial l \simeq \left(\partial U^{(1)}/\partial y\right)\left(\partial y_s/\partial x\right)=\left(\partial U^{(1)}/\partial y\right)\left(\partial h/\partial x\right).$$

On the other hand, since the electric field acts only in the normal direction at the interface, there is no component of the electric force in the tangential direction and (30) is expected to hold as a first approximation. Accordingly, the electric field is assumed to have only a passive effect on the surfactant transport. The linearized kinematic

equation at the interface has the form

$$\frac{\partial \psi^{(1)}}{\partial x} + U^{(1)} \frac{\partial h}{\partial x} + \frac{\partial h}{\partial t} = 0. \tag{31}$$

The continuity of the normal and the tangential components of the velocity at the interface gives

$$\frac{\partial \psi^{(2)}}{\partial x} - \frac{\partial \psi^{(1)}}{\partial x} + \left(U^{(2)} - U^{(1)}\right) \frac{\partial h}{\partial x} = 0, \tag{32}$$

$$\frac{\partial \psi^{(2)}}{\partial y} - \frac{\partial \psi^{(1)}}{\partial y} = 0. \tag{33}$$

Also, for the electric field, the continuity of the normal and the tangential components at the interface gives

$$\frac{\partial \phi_p^{(1)}}{\partial y} - \hat{\varepsilon} \frac{\partial \phi_p^{(2)}}{\partial y} = 0, \quad \hat{\varepsilon} = \varepsilon^{(2)} / \varepsilon^{(1)}, \tag{34}$$

$$\frac{\partial \phi_p^{(1)}}{\partial x} - \frac{\partial \phi_p^{(2)}}{\partial x} + \left(\frac{\partial \phi_b^{(1)}}{\partial y} - \frac{\partial \phi_b^{(2)}}{\partial y} \right) \frac{\partial h}{\partial x} = 0. \tag{35}$$

In addition the perturbed electric potential is zero at the two plates, i.e. $\phi_p^{(1)} = 0$ at $y = 0$ and $\phi_p^{(2)} = 0$ at $y = 1$. Beside the Reynolds number R_e there are three important dimensionless numbers involved in the dynamic boundary conditions above, which are the Marangoni number $M_a = E\Gamma_0 / \gamma_0$, expressing the sensitivity of the surface and interfacial tensions on the surfactant concentrations, the capillary number $C_a = \mu^{(1)} U_c / \gamma_0$ measuring the relative strength of the viscous and surface tension forces, and the electric Weber number $W_e = \varepsilon^{(1)} E_0^2 h_2 / \left(\mu^{(1)} U_c \right)$, which measures the ratio of electrical to viscous forces.

Differential Eqs. (21) and (26) along with boundary conditions (27)-(35) completely specify the stability problem for the two film flow configuration of interest in this study. For arbitrary R_e and k, there are no closed form solutions to the fourth-order differential Eq. (26), and so a numerical method must be used to solve the stability problem in general. Thus we will deal with this equation in two cases, the first is the case of low Reynolds number i.e. $R_e \ll 1$, in which that the inertial forces will be small compared to the viscous forces (which is known by Stokes approximation). The second is the long waves evolution, in which we consider low wave number $k \ll 1$, thus an asymptotic analysis in the small parameter k is possible, which yields an analytical expression for the wave speed as an asymptotic series in k Shankar and Kumar (2004). In the following section, we briefly out-line the low wavenumber asymptotic analysis and the results obtained from that analysis.

The general solution of Orr-Sommerfeld Eq. (26) in the limit of Stokes flow ($R_e \to 0$) has the form

$$\begin{aligned} \hat{\psi}^{(r)} = {} & A_1^{(r)} \cosh ky + A_2^{(r)} \sinh ky \\ & + A_3^{(r)} y \cosh ky + A_4^{(r)} y \sinh ky. \end{aligned} \tag{36}$$

Further, by substituting the form of Eq. (24) for $\phi^{(r)}$ into Eq. (21), the yields equation has the general solution

$$\phi^{(r)} = B_1^{(r)} \cosh ky + B_2^{(r)} \sinh ky, \tag{37}$$

where the coefficients $A_1^{(r)}, A_2^{(r)}, A_3^{(r)}, A_4^{(r)}, B_1^{(r)}$ and $B_2^{(r)}$ are constants of integration which will be determined after satisfying the above boundary and interface conditions.

3.1 Derivation of the Characteristic Equation

In this section, we will derive the dispersion relation controlling the stability behavior of the system. When the obtained solutions of the stream function and electric potential are inserted into Eqs. (27)-(35), we have a linear homogeneous system of algebraic equations of fourteen unknown coefficients. This homogeneous system of equations can be expressed in a matrix form as

$$\mathbf{AX=0}, \tag{38}$$

where **0** is a null vector, **X** is a vector of unknown coefficients defined as

$$\begin{aligned} \mathbf{X}^{Tr} = \Big(& A_1^{(1)},\ A_2^{(1)},\ A_3^{(1)},\ A_4^{(1)},\ A_1^{(2)},\ A_2^{(2)},\ A_3^{(2)}, \\ & A_4^{(2)}, B_1^{(1)},\ B_2^{(1)},\ B_1^{(2)},\ B_2^{(2)},\ \hat{h},\ \hat{\Gamma} \Big), \end{aligned} \tag{39}$$

and **A** is the coefficient matrix, whose rows represent the different interface and boundary conditions, given by

$$\begin{pmatrix}
1 & 0 & 0 & 0 & 0 & 0 & 0 \\
0 & 0 & 0 & 0 & C_k & S_k & C_k \\
0 & k & 1 & 0 & 0 & 0 & 0 \\
0 & 0 & 0 & 0 & kS_k & kC_k & C_k + kS_k \\
C_{\hat{k}} & S_{\hat{k}} & h_0 C_{\hat{k}} & h_0 S_{\hat{k}} & -C_{\hat{k}} & -S_{\hat{k}} & -h_0 C_{\hat{k}} \\
kS_{\hat{k}} & kC_{\hat{k}} & C_{\hat{k}} + kS_{\hat{k}} & S_{\hat{k}} + \hat{k}C_{\hat{k}} & -kS_{\hat{k}} & -kC_{\hat{k}} & -C_{\hat{k}} - \hat{k}S_{\hat{k}} \\
kS_{\hat{k}} & kC_{\hat{k}} & C_{\hat{k}} & \hat{k}S_{\hat{k}} & S_{\hat{k}} & \hat{k}C_{\hat{k}} & 0 \\
kC_{\hat{k}} & kS_{\hat{k}} & \hat{k}C_{\hat{k}} & \hat{k}S_{\hat{k}} & 0 & 0 & 0 \\
kC_{\hat{k}} & kS_{\hat{k}} & S_{\hat{k}} + \hat{k}C_{\hat{k}} & C_{\hat{k}} + \hat{k}S_{\hat{k}} & -k\hat{\mu}^{(2)} C_{\hat{k}} & -k\hat{\mu}^{(2)} S_{\hat{k}} & -\hat{\mu}^{(2)} \left(S_{\hat{k}} + \hat{k}C_{\hat{k}} \right) \\
kS_{\hat{k}} & kC_{\hat{k}} & \hat{k}S_{\hat{k}} & \hat{k}C_{\hat{k}} & -k\hat{\mu}^{(2)} S_{\hat{k}} & -k\hat{\mu}^{(2)} C_{\hat{k}} & -\hat{k}\hat{\mu}^{(2)} S_{\hat{k}} \\
0 & 0 & 0 & 0 & 0 & 0 & 0 \\
0 & 0 & 0 & 0 & 0 & 0 & 0 \\
0 & 0 & 0 & 0 & 0 & 0 & 0 \\
0 & 0 & 0 & 0 & 0 & 0 & 0
\end{pmatrix}$$

$$\begin{pmatrix}
0 & 0 & 0 & 0 & 0 & 0 & 0 \\
S_k & 0 & 0 & 0 & 0 & 0 & 0 \\
0 & 0 & 0 & 0 & 0 & 0 & 0 \\
kC_k + S_k & 0 & 0 & 0 & 0 & 0 & 0 \\
-h_0 S_{\hat{k}} & 0 & 0 & 0 & 0 & 0 & \tilde{h} \\
-\hat{k}C_{\hat{k}} & 0 & 0 & 0 & 0 & 0 & 0 \\
0 & 0 & 0 & 0 & 0 & \tilde{\Gamma} - c & a_1^{(1)} - h_0 \\
0 & 0 & 0 & 0 & 0 & 0 & k\left(\tilde{\Gamma} - c\right) \\
-\hat{\mu}^{(2)}\left(C_{\hat{k}} + \hat{k}S_{\hat{k}}\right) & 0 & 0 & 0 & 0 & \frac{iM_a}{2C_a} & 0 \\
-\hat{k}\hat{\mu}^{(2)}C_{\hat{k}} & -ikE_f S_{\hat{k}} & -ikE_f C_{\hat{k}} & ikE_f S_{\hat{k}} & ikE_f C_{\hat{k}} & 0 & \frac{ik}{2C_a} + \breve{h} \\
0 & 1 & 0 & 0 & 0 & 0 & 0 \\
0 & 0 & C_{\hat{k}} & S_{\hat{k}} & 0 & 0 & 0 \\
0 & -C_{\hat{k}} & -S_{\hat{k}} & C_{\hat{k}} & S_{\hat{k}} & 0 & \frac{2k\left(\hat{\varepsilon} - 1\right)E_f}{\hat{\varepsilon}W_e} \\
0 & S_{\hat{k}} & C_{\hat{k}} & -\hat{\varepsilon}S_{\hat{k}} & -\hat{\varepsilon}C_{\hat{k}} & 0 & 0
\end{pmatrix} \tag{40}$$

where

$C_k = \cosh k,\ S_{\hat{k}} = \sinh \hat{k},\ C_{\hat{k}} = \cosh \hat{k},\ S_k = \sinh k,$

$\hat{k} = kh_0,$

$$\tilde{h} = a_1^{(1)} - a_2^{(2)} - \frac{1}{2k}\left(1 - \hat{\rho}^{(2)}\right)\cot\beta + \frac{\hat{k}}{2k}\left\{2a_1^{(1)} - 2a_1^{(2)} + \frac{\hat{k}}{2k}\left(\hat{\rho}^{(2)}/\hat{\mu}^{(2)} - 1\right)\right\},$$

$$\tilde{\Gamma} = a_2^{(1)} + \frac{\hat{k}}{k}a_1^{(1)} - \frac{\hat{k}^2}{2k^2},\quad \breve{h} = a_1^{(1)} - a_1^{(2)}\hat{\mu}^{(2)} + \frac{\hat{k}}{k}\left(\hat{\rho}^{(2)} - 1\right), E_f = \frac{\hat{\varepsilon}W_e\phi_0}{2k + 2\left(\hat{\varepsilon} - 1\right)\hat{k}}.$$

A non-trivial solution of the above unknown quantities of the system (40) exists if and only if the determinant of the 14 × 14 matrix A coincides with zero, which yields a dispersion relation between the wavenumber k and the perturbation frequency *c* for specified values of other parameters, given by

$$D\left(c, k; M_a, C_a, W_e, \hat{\rho}^{(2)}, \hat{\mu}^{(2)}, \hat{\varepsilon}, \phi_0\right) = 0, \tag{41}$$

which represents the linear dispersion equation for surface waves propagating through the boundary embedded between two other fluids with the influence of constant perpendicular electric field. This dispersion relation controls the stability in the present problem. That is, each imaginary part of c which assumes a negative sign will give a stable mode of the interfacial disturbance. On the other hand, if the imaginary part of c is positive, the disturbance will grow in time and the flow becomes unstable.

3.2 Numerical Results

In the current analysis, we deal with the stability diagrams in the limit case of Stokes flow, where the dispersion Eq. (41) is utilized to control the stability behavior. The stability of fluid film corresponds to negative values of the disturbance growth rate (i.e. $c_i < 0$), and the disturbance growth rates of the flow can be gained through solving the above corresponding dispersion relation numerically. Fortunately, the disturbance growth rates can be gained through solving the above corresponding dispersion equation numerically with the aid of Mathematica that enable us to plot the imaginary part of c_i without solving the equation. Hence, we are able to produce graphs depending on the growth rate behavior, illustrating how these parameters depending on the other dimensionless quantities.

Now, to investigate the effect of both surfactants and surface tension, we computed numerical solutions of the above dispersion equation for nonzero values of the Marangoni and capillary numbers, through the parts of Fig. 2. The concept of the critical wave number to study the stability, which separates the stable motions from the unstable ones and conversely Liu (1998). In addition, physically reasonable values of the non-dimensional parameters are selected to analyze the results Blyth and Pozrikidis (2004), Blyth (2008), Mikishev and Nepomnyashchy (2010), Yiantsios and Higgins (2010), Sirwah (2012), Uma and Usha (2012); Park *et al*. (2013). The part (a) of Fig. 2 shows the variation of the non-dimensional growth rate ci with the non-dimensional wave number *k* for a system having the parameters given in the caption of Fig. 2. In this figure the continuous line represents the value 1 of the Marangoni number, the dashed curve denotes the value M_a = 2, and the dotted line corresponds to M_a = 3. One can see from this graph that the areas above the wave number axis (i.e. the range to the left of the critical wave numbers) and below the curves assume unstable regions, because of the positive sign of the imaginary part of the complex frequency, while the regions below the wave number axis (i.e. the range right to the critical wave numbers) which represent the negative values of the disturbance growth rate, are stable. In this sense, we deduce that the growth rate is decreased due to increase of the Marangoni number, where we have three critical wave numbers which are 0.52, 0.45, and 0.41 corresponding to the values 1, 2, and 3 of M_a respectively. Thus, it is obvious that as the Marangoni number increases both the growth rate and the cutoff wave numbers decrease, and hence we conclude that the Marangoni number has a stabilizing influence on the movement of the films, which means that the inertialess stability of the flow is enhanced by the presence of the interfacial surfactant. The two parts (b) and (c) of Fig. 2 are illustrated at the values 0.5 and 0.7 for the capillary number to show the response of the flow. The inspection of the parts for Fig. 2 indicates that as the capillary number is increased both the growth rates and the critical wave numbers are enhanced, or alternatively that the unstable regions under the curves are extended. Having checked the stability picture of this figure, it is discovered that increasing the capillary number leads to a growth of the instability areas above the wave number axis, and consequently the capillary number has a destabilizing influence in the fluid flow. A general conclusion of Fig. 2 is that the Marangoni number and the capillary number have an opposite effect on the movement of the wave, this opposite influence is expected from the obtained dispersion relation of the current problem.

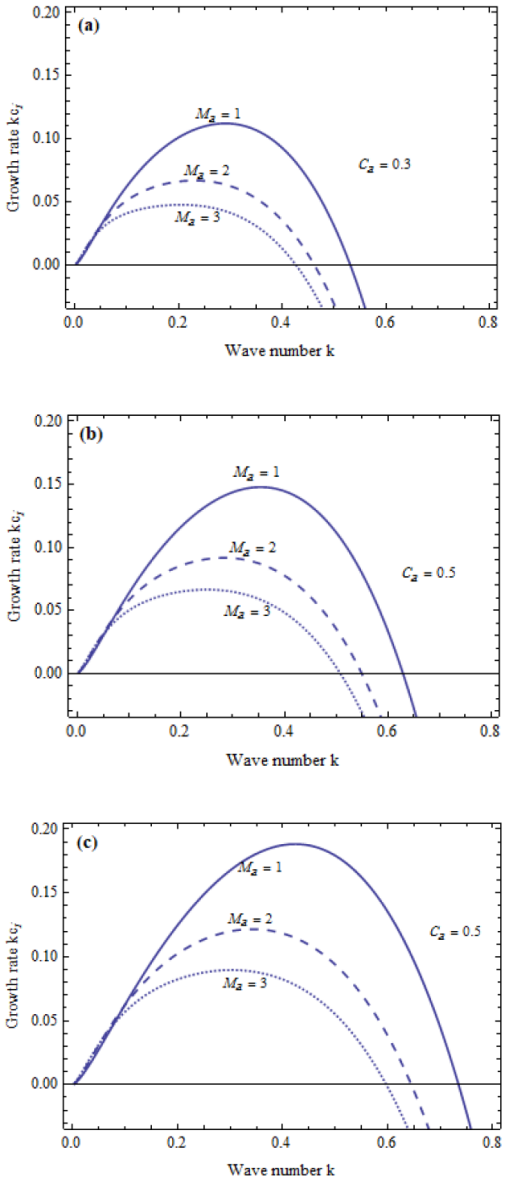

Fig. 2. Effect of the interfacial surfactant through the Marangoni number, on the inertialess stability for $\hat{\mu}^{(2)} = 0.4, \hat{\rho}^{(2)} = 0.5$, $\hat{\varepsilon} = 0.6, W_e = 1.5, h_0 = 0.5, f_0 = 0.9$, $\beta = \pi/9$ where, M_a=1 (solid curve), 2 (dashed line), 3 (dotted curve), with C_a = 0.3, 0.5 and 0.7 of the partitions (a), (b) and (c), respectively.

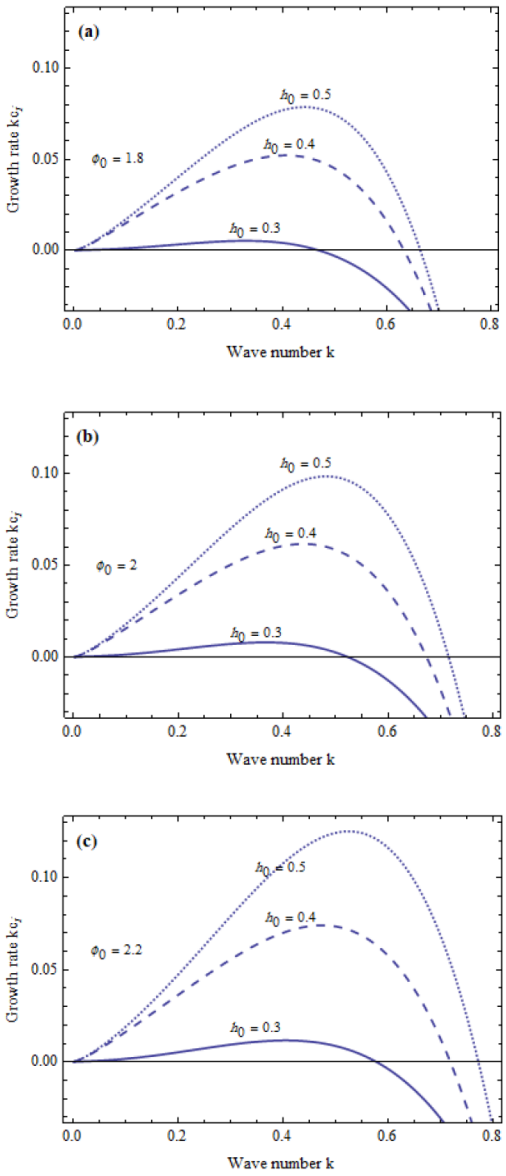

Fig. 3. The stability diagrams in the plane ($kc_i - k$), for the same system in Fig. 2, with M_a = 2, where h_0=0.3 (solid curve), 0.4 (dashed line), 0.5 (dotted curve) whereas the values $f_0 = 1.8$, $f_0 = 2$, and $f_0 = 2.2$ are selected for the parts (a), (b) and (c), respectively.

Figure 3a is the plot of the wave number *k* versus the growth rate ci for different values of the thickness ratio $h_0 = h_1/ h_2$, when the constant electric potential $\phi_0 = 1.8$, the aim here is to examine the influence of fluid thickness and electric potential on the stability behavior of the motion of the waves. The values of other parameters are fixed, as specified in the caption of Fig. 2. The inspection of the stability of this diagrams reveals that there are three critical wave numbers given by 0.47, 0.6, and 0.67, matching the values 0.3, 0.4,and 0.5 of h_0, respectively.

Thus, it is obvious that as the thickness ratio increases both the growth rate and the critical wave numbers increase, and hence we conclude that the thickness ratio has a destabilizing influence. The increasing of the electric potential to the value $\phi_0 = 2$ under the same values of the other parameters is given in Fig. 3(b). The stability diagram that is shown in this graph illustrates that the unstable regions below the curves increase. More extension is observed in the unstable areas under the growth rate lines, this due is to more increasing in the electric potential $\phi_0 = 2.2$ through the part (c) of Fig. 3. By comparing the partitions (a), (b) and (c) of this figure, it was found that both the peak growth rate and the critical wave number

increased as the electric potential ϕ_0 increased. The electric potential thus has a destabilizing effect on the interface between the two fluids for the selected values of input parameters. In other words for a fixed value of electric potential, the system is unstable for a wave number less than the critical wave number after which the system is stable.

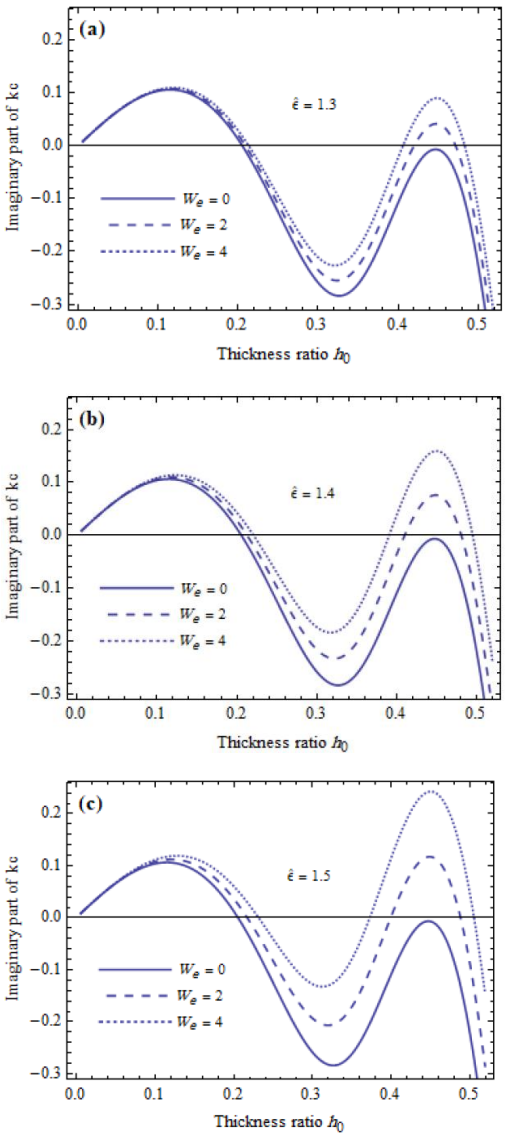

Fig. 4. Stability boundaries of the variation of the dielectric constant ratio and the electric Weber number on the stability picture in the plane ($kc_i - h_0$): part (a) at $\hat{\varepsilon} = 1.3$, (b) at $\hat{\varepsilon} = 1.4$, (c) at $\hat{\varepsilon} = 1.5$.

The examination of the increase of the dielectric constant ratio $\hat{\varepsilon} = \varepsilon^{(2)} / \varepsilon^{(1)}$ and the electric Weber number on the wave growth rate is displayed in the plane ($kc_i - h_0$) through the parts (a-c) of Fig. 4. The calculations are made for a system having the same parameters given in Fig. 2 with k = 0.5, while the dielectric constants ratio and the Weber number have some variation for the sake of comparison. In part (a) of this graph, the solid line represents the value zero of the Weber number, the value W_e = 2 corresponds to the dashed curve and the dotted curve is plotted at the value W_e = 4. Inspection of the stability diagrams of Fig. 4(a) reveals that the system under the effect of the given parameters represents unstable mode in the range $0 < h_0 < 0.2$. In addition, it is to be noted that both of the electric Weber number and the dielectric constants ratio has an effect on the growth rate when the thickness ratio less than the value 0.1 and further there is a slight influence in the range $0.1 < h_0 < 0.2$. On the other hand, the system is stable for all values in the range $0.2 < h_0 < 0.4$ after which the system becomes unstable. A general trend revealed here is that the phenomenon of the dual (irregular) role is observed for increasing electric Weber number: one of the two roles is a stabilizing influence in the range $0.2 < h_0 < 0.4$, and the others are destabilizing influence in the ranges $0 < h_0 < 0.2$ and $0.4 < h_0 < 0.5$. A comparison of the parts a, b and c of Fig. 4, where it is plotted respectively at the values $\hat{\varepsilon}$ = 1.3, 1.4 and 1.5, shows that broadly speaking, the ratio between the dielectric constants $\varepsilon^{(2)}$ and $\varepsilon^{(1)}$ has a principle role in the administration of the behavior of the electric field. This suggests that when the dielectric constant of the upper fluid $\varepsilon^{(2)}$ is more than its counterpart of the lower fluid $\varepsilon^{(1)}$, the field transmits a part of the kinetic energy to the interfacial waves, which leads to instability of the motion ofwaves.

The influence of the density and the viscosity ratios on the stability behavior in the plane ($kc_i - h_0$) is presented throughout the parts of Fig. 5 for a system having the same parameters considered in Fig. 2. In this graph, three distinct values of the density ratio and the viscosity ratio are selected for the sake of comparison. In which, the values 0.5, 1, and 1.5 are chosen for the ratio correspond to the solid, dashed, and dotted curves respectively, whereas the upper to the lower density ratio $\hat{\rho}^{(2)}$ has respectively the values 0.5, 0.9 and 1.4 for the parts (a), (b) and (c) of Fig. 5. It is observed that from part (a) of Fig. 5, there are two modes of instability behavior separated by the value 0.5 of the thickness ratio. Before this value, we found that an increasing of the ratio $\hat{\mu}^{(2)}$ leads to decrease the growth rate, when the range exceed h_0 = 0.5 an increment of the viscosity ratio leads to an extension in the instability areas under the curves, indicating that increasing the viscosity ratio results in an increasing growth rate of disturbances on the fluids, which destabilizes the fluid sheets. Hence the phenomenon of the dual role is found for increasing the upper to the lower viscosity ratio, which has two roles, one is a stabilizing influence in the range $0 < h_0 < 0.5$ and the other is a destabilizing influence when the ratio $h_0 \in (0.5,1)$.

On the other hand, the comparison of the three parts of Fig. 5, shows that, in the range when h_0 is less than 0.5, the increasing of the density ratio has a digitalizing effect, in which there are increases in both growth rate and the unstable regions. In addition, it important to note that the density ratio has no effect on the stability conditions when the thickness ratio is contained between the two values

0.5 and 1. A similar result was reported by Ozen *et al.*(2006), in their studies of the electrohydrodynamic linear stability of two immiscible fluids in channel flow.

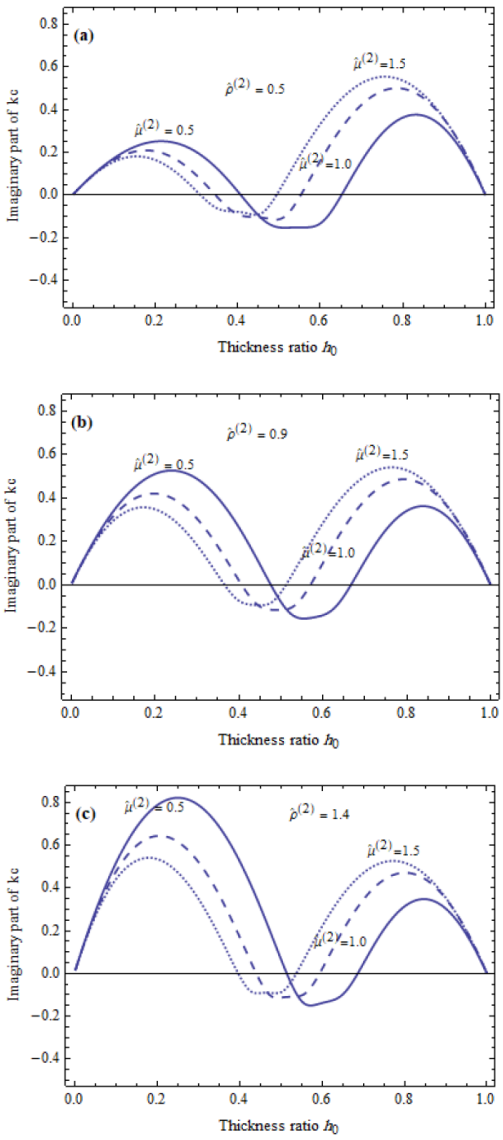

Fig. 5. The growth rate kc_i as a function of the thickness ratio h_0, for the same system considered in Fig. 2, with k = 0.5, where $\hat{\mu}^{(2)}$ =0.5 (solid curve), 1 (dashed line), 1.5 (dotted curve) whereas the values $\hat{\rho}^{(2)}$ = 0.5, 0.9 and 1.4 are selected for the parts (a), (b) and (c), respectively.

4. EVOLUTION OF LONG WAVES

Once more, we return to the general form of the system (26)-(33) governs the linear stability problem, in which the effect of the Reynolds number on the stability of the two layers is considered. For finite wavelength instabilities, the differential system should be solved numerically, while long-wavelength solutions can be analytically obtained by an expansion in $k \ll 1$. So the differential equation governing the leading order and first correction to the stream velocity is solved analytically and will be discussed in this section.

Using a regular perturbation expansion, the appropriate long wave expansions for the quantities $\hat{\psi}^{(r)}$ and $\phi_p^{(r)}$ are express as

$$f^{(r)}(y) = f_0^{(r)}(y) + k f_1^{(r)}(y), \tag{42}$$

and also we can write

$$c = c_0 + k c_1, \tag{43}$$

$$\left\{\hat{h}, \hat{\Gamma}\right\} = \left\{\hat{h}_0, 1\right\} + k\left\{\hat{h}_1, \hat{\Gamma}_1\right\}. \tag{44}$$

Implementing the regular perturbation method, by substituting these expansions into Eqs. (21), (26) and the corresponding boundary conditions, and grouping the terms of equal order in k, we obtain the following ordered problems and their solutions. At order $O(1)$

$$\frac{d^4\hat{\psi}_0^{(r)}}{dy^4} = 0, \text{ and } \frac{d^4\phi_{0p}^{(r)}}{dy^2} = 0, \tag{45}$$

which have the solutions

$$\begin{aligned} \hat{\psi}_0^{(r)} &= A_{01}^{(r)} y^3 + A_{02}^{(r)} y^2 + A_{03}^{(r)} y + A_{04}^{(r)}, \\ \phi_{0p}^{(r)} &= B_{01}^{(r)} y + B_{02}^{(r)}, \end{aligned} \tag{46}$$

subjected to the following conditions

$$\hat{\psi}_0^{(r)} = \frac{d^2\hat{\psi}_0^{(r)}}{dy^2} = 0, \text{ at } y = r\text{-}1, \tag{47}$$

$$\hat{\psi}_0^{(2)} - \hat{\psi}_0^{(1)} + \left(U^{(2)} - U^{(1)}\right)\hat{h}_0 = 0, \text{ at } y = h_0, \tag{48}$$

$$\frac{d\hat{\psi}_0^{(2)}}{dy} - \frac{d\hat{\psi}_0^{(1)}}{dy} = 0, \text{ at } y = h_0, \tag{49}$$

$$\frac{d\hat{\psi}_0^{(1)}}{dy} + \hat{h}_0\frac{dU^{(1)}}{dy} + U^{(1)} - c_0 = 0, \text{ at } y = h_0, \tag{50}$$

$$\hat{\psi}_0^{(1)} + \hat{h}_0\left(U^{(1)} - c_0\right) = 0, \text{ at } y = h_0, \tag{51}$$

$$\frac{d^2\hat{\psi}_0^{(1)}}{dy^2} - \hat{\mu}^{(2)}\frac{d^2\hat{\psi}_0^{(2)}}{dy^2} = 0, \text{ at } y = h_0, \tag{52}$$

$$\frac{d^3\hat{\psi}_0^{(1)}}{dy^3} - \hat{\mu}^{(2)}\frac{d^3\hat{\psi}_0^{(2)}}{dy^3} = 0, \text{ at } y = h_0, \tag{53}$$

and the electric potential conditions are

$$\phi_{0p}^{(r)} = 0, \text{ at } y = r\text{-}1 \tag{54}$$

$$\phi_{0p}^{(2)} - \phi_{0p}^{(1)} + \hat{h}_0\left(\phi_b^{(2)} - \phi_b^{(1)}\right) = 0 \text{ at } y = h_0, \tag{55}$$

$$\frac{d\phi_{0p}^{(1)}}{dy}-\hat{\varepsilon}\frac{d\phi_{0p}^{(2)}}{dy}=0,\ \text{at}\ \ y=h_0, \tag{56}$$

By substituting Eq. (46) into these conditions, we obtain the constants that appear in Eq. (46), further the values of the quantities $\hat{h}_0$ and c_0. For the two film configuration in the presence of insoluble surfactants is of interest in this work, our asymptotic analysis shows that at leading order, c_0 is purely real, and is identical to the results by Shankar and Kumar (2004), which result for leading order wave speed in the two-layer plane Couette flow of Newtonian fluids in a rigid channel. In other words, the normal stress differences between the two fluids and the effect of surfactants do not appear at the leading order problem in the present study. Thus, in order to determine the stability of the system, one must calculate the first correction c1, which is obtained by solving the problem at order $O(k)$:

$$\begin{aligned}&\frac{d^4\hat{\psi}_1^{(r)}}{dy^4}+\frac{iR_e\hat{\rho}^{(r)}}{\hat{\mu}^{(r)}}\left\{\left(c_0-U^{(r)}\right)\frac{d^2\hat{\psi}_0^{(r)}}{dy^2}\right.\\&\left.+\frac{d^2U^{(r)}}{dy^2}\hat{\psi}_0^{(r)}\right\}=0\ \ \text{and}\ \ \frac{d^2\phi_{1p}^{(1)}}{dy^2}=0,\end{aligned} \tag{57}$$

which have the solutions

$$\begin{aligned}\hat{\psi}_1^{(r)}&=A_{11}^{(r)}y^3+A_{12}^{(r)}y^2+A_{13}^{(r)}y+A_{14}^{(r)}\\&-\frac{iR_e\hat{\rho}^{(r)}y}{\hat{\mu}^{(r)}}\left\{\frac{\hat{\rho}^{(r)}}{420\hat{\mu}^{(r)}}A_{01}^{(r)}y^6-\frac{a_1^{(r)}A_{01}^{(r)}}{60}y^5\right.\\&+\frac{1}{120}\left[6\left(c_0-a_2^{(r)}\right)A_{01}^{(r)}-2a_1^{(r)}A_{02}^{(r)}-\frac{\hat{\rho}^{(r)}}{\hat{\mu}^{(r)}}A_{03}^{(r)}\right]y^4\\&+\frac{1}{24}\left[2\left(c_0-a_2^{(r)}\right)A_{02}^{(r)}-\frac{\hat{\rho}^{(r)}}{\hat{\mu}^{(r)}}A_{04}^{(r)}\right]y^3\\&\left.+\frac{1}{6}\left[\left(c_0-2a_2^{(r)}\right)A_{03}^{(r)}-2a_1^{(r)}A_{04}^{(r)}\right]y^2+\frac{1}{2}c_0A_{04}^{(r)}y\right\},\end{aligned} \tag{58}$$

$$\phi_{1p}^{(r)}=B_{11}^{(r)}y+B_{12}^{(r)}. \tag{59}$$

To determine the constants in these equations the following conditions are achieved, where at the plates we have

$$\hat{\psi}_1^{(r)}=\frac{d^2\hat{\psi}_1^{(r)}}{dy^2}=0\ \ \text{at}\ y=r\text{-}1, \tag{60}$$

and at the interface we get

$$\hat{\psi}_1^{(2)}-\hat{\psi}_1^{(1)}+\left(U^{(2)}-U^{(1)}\right)\hat{h}_1=0, \tag{61}$$

$$\frac{d\hat{\psi}_1^{(2)}}{dy}-\frac{d\hat{\psi}_1^{(1)}}{dy}=0, \tag{62}$$

$$\frac{d\hat{\psi}_1^{(1)}}{dy}+\hat{h}_1\frac{dU^{(1)}}{dy}+\left(U^{(1)}-c_0\right)\hat{\Gamma}_1-c_1=0, \tag{63}$$

$$\hat{\psi}_1^{(1)}+\left(U^{(1)}-c_0\right)\hat{h}_1-\hat{h}_0c_1=0, \tag{64}$$

$$\frac{d^2\hat{\psi}_1^{(1)}}{dy^2}-\hat{\mu}^{(2)}\frac{d^2\hat{\psi}_1^{(2)}}{dy^2}+i\frac{M_a}{C_a}=0, \tag{65}$$

$$\begin{aligned}&\frac{d^3\hat{\psi}_0^{(1)}}{dy^3}-\hat{\mu}^{(2)}\frac{d^3\hat{\psi}_0^{(2)}}{dy^3}+iR_e\left\{\frac{dU^{(1)}}{dy}\hat{\psi}_0^{(1)}\hat{\rho}^{(2)}\right.\\&\left.-\frac{dU^{(1)}}{dy}\hat{\psi}_0^{(1)}\right\}+iR_e\left(c_0-U^{(1)}\right)\frac{d\hat{\psi}_0^{(1)}}{dy}\\&-iR_e\hat{\rho}^{(2)}\left(c_0-U^{(2)}\right)\frac{d\hat{\psi}_0^{(2)}}{dy}-i\hat{h}_0\left(1-\hat{\rho}^{(2)}\right)\cot\beta\\&-iW_e\left\{\frac{d\phi_b^{(1)}}{dy}\frac{d\phi_{0p}^{(1)}}{dy}-\hat{\varepsilon}\frac{d\phi_b^{(2)}}{dy}\frac{d\phi_{0p}^{(2)}}{dy}\right\}=0,\end{aligned} \tag{66}$$

and the conditions for the electric potential read

$$\phi_{1p}^{(r)}=0\ \text{at}\ y=r\text{-}1, \tag{67}$$

$$\phi_{1p}^{(2)}-\phi_{1p}^{(1)}+\hat{h}_1\left(\phi_b^{(2)}-\phi_b^{(1)}\right)=0,\ \text{at}\ y=h_0, \tag{68}$$

$$\frac{d\phi_{1p}^{(1)}}{dy}-\hat{\varepsilon}\frac{d\phi_{1p}^{(2)}}{dy}=0,\ \text{at}\ y=h_0. \tag{69}$$

Beside these conditions, since the perturbations are assumed small, we can express the relation between complex amplitudes $\hat{h}_1$ and $\hat{\Gamma}_1$ by the equation $\hat{h}_1=-M_a\hat{\Gamma}_1$. Thus the above conditions are sufficient to determine all constants in Eqs. (48) and (49), in addition, the values of the parameters $\hat{h}_1$ and $\hat{\Gamma}_1$, further the value of c_1. The mathematical formulas of these constants are lengthy and not included here. However, they are available upon request from the authors. On the other hand, the quantity c_1 is purely imaginary (Shankar and Kumar (2004)) and used to describe the stability process in the case of the long wave assumption. That is, if the imaginary part of c_1, $Im(c_1)$, is negative, a stable long wave is obtained, while for each positive value $Im(c_1)$ the disturbance will grow in time and the long wave flow becomes unstable. In addition when $Im(c_1)$ equal zero the neutral stability arises. Consequently, the system will be neutrally stable when $c_{1i}=0$, this condition leads to three equations for the critical values R_{ec}, C_{ac} and ϕ_{0c}, which can take the form

$$L_1\left(F_1;R_e,C_a,\phi_0\right)F_c+L_2\left(F_2;R_e,C_a,\phi_0\right)=0, \tag{70}$$

where, the quantity F_c will express the critical values of R_{ec}, C_{ac} or ϕ_{0c}, while L_1, L_2 are functions of the others physical parameters. This equation

will be used to produce graphs illustrating how these parameters depending on the other dimensionless quantities.

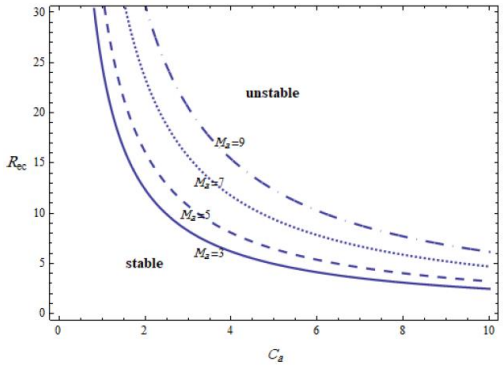

Fig. 6. Influence of the Marangoni number on the neutral stability diagrams in the case of long wave limit in the plane ($R_{ec}-C_a$), for a system having the parameters

$$\hat{\mu}^{(2)}=0.4,\hat{\rho}^{(2)}=1.5,\hat{\varepsilon}=0.8,W_e=2,h_0=0.3,\phi_0=0.9,$$

with M_a=3, 5, 7 and 9.

In what follows, to understand the flow characteristics on the stability behavior of the long wave limit, the conditions obtained by linear long wave stability analysis are numerically evaluated for different values of the four dimensionless numbers considered in this work, which are Marangoni, Reynolds, electric Weber and capillary numbers.

The stability diagrams in Fig. 6 illustrates the neutral stability curves for the behavior of the critical Reynolds number R_{ec} independent on the capillary number C_a for several values of the Marangoni number. Each curve in this graph separates the zones of stability (below the curves) and instability (upper the curves). It is worth mentioning to observe that the increase of M_a values leads to a shrinkage of the region of unstable long wave, which in turn confirms the significantly stabilizing influence of Marangoni number. On the other hand, in view of the horizontal axis of the capillary number, it obvious that at any one of the four neutral curves, when the capillary number increases, this leads to an extension in the unstable area above the curve, which confirms the destabilizing influence of the capillary number obtained before in the case of Stokes flow. The converse relation between the effect of capillary and Marangoni numbers is also cleared.

In Fig. 7, the behavior of the critical capillary number is illustrated as a function of the dielectric constant ratio for several values of the Reynolds number at the same system considered in Fig. 6. It is clear that the increase of Reynolds number values leads to a shrinkage of the region of stable long wave, which shows that the Reynolds number still acquires a destabilizing effect on the motion of the interfacial waves based on the selected values of the physical parameters, thus confirms the significantly stabilizing influence of viscosity coefficient of the lower layer flow. In addition, we can observe that as the dielectric constants ratio increases along the horizontal axis, the Reynolds number grow through the neutral curves, which means that both the Reynolds number and the dielectric constants ratio has the same destabilizing influence on the movement of the surface waves.

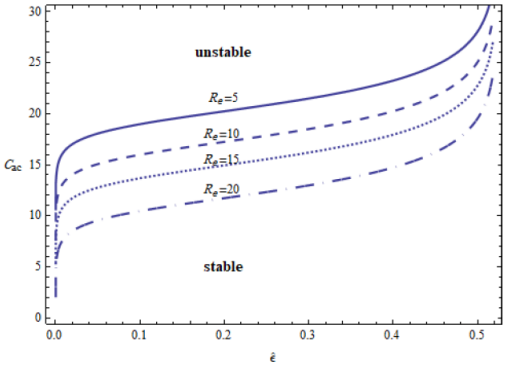

Fig. 7. Neutral stability curves in the plane $(C_{ac}-\hat{\varepsilon})$, for a system having the same physical parameters as considered in Fig. 6: the stability criteria due to the variation of R_e=5, 10, 15 and 20.

Figure 8 represents the neutral stability curves in the plane $(C_{ac}-\hat{\varepsilon})$ for the same system as considered in Fig. 6, when the values of the electric Weber number are increased stepwise from 1 to 7 for the sake of comparison. It is observed that increasing the electric Weber number results in decreasing the stable areas under the curves, which destabilizes the long wave.

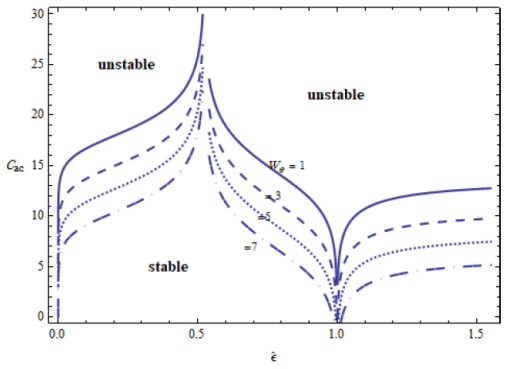

Fig. 8. Critical capillary number C_a for long wave versus the dielectric constant ratio $\hat{\varepsilon}$, for different values of W_e=1, 3, 5 and 8.

Furthermore, the dielectric constants ratio axis is divided into three ranges, the first when $\hat{\varepsilon}$ has the range (0,0.5), the second is the domain $0.5 < \hat{\varepsilon} < 1$ and the third range when $\hat{\varepsilon}$ greater than the value 1. The inspection of these intervals reveals that in the middle interval as the dielectric constants ratio increases the critical capillary number C_{ac} decreases, where it is increasing on the other ranges due to the increases in the dielectric constants ratio.

Thus we can say that the phenomenon of the dual influence on the stability case is found to the dielectric constants ratio when the long wave approximation is taken into account.

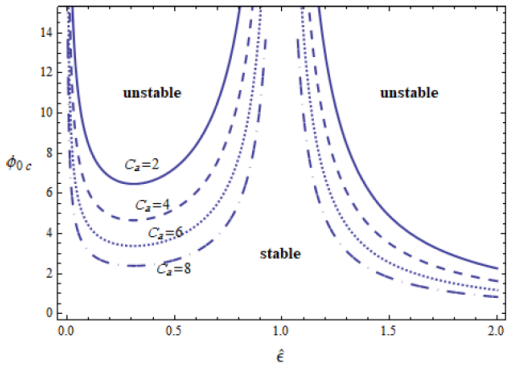

Fig. 9. Variation of the critical electrical potential versus the dielectric constant ratio for a system having the same parameters as considered in Fig. 6: C_a=2, 4, 6, 8.

The stability limit is presented in Fig. 9, where the critical electric potential is plotted versus the dielectric constants ratio for different values of the capillary number. In this figure the solid curve is plotted at the value C_a = 2 and the value C_a = 4 corresponds to the dashed line, while the dotted curve represents the value C_a = 6, whereas the dotted-dashed curve is plotted at C_a = 8. From this graph, it is observed that increasing the capillary number results in decreasing both the critical electric potential and the stable zones, this shows that the two films become less stable as C_a increases, which confirm the destabilizing influence of the capillary number illustrated in Fig. 6 before. It is worth mentioning to observe that the dielectric constants ratio has no effect in the range $\hat{\varepsilon} \in (0.85,1.2)$, while it has a significant influence at large values of the critical electric potential.

5. CONCLUSIONS

A linear stability study of two viscous films channel flow bounded by two infinite parallel plates, with an insoluble surfactant along the interface and in the presence of normal electric field is carried out. Two Orr-Sommerfeld equations for the perturbed vertical components of velocity in the two fluids are obtained. These equations together with boundary conditions at the plates and the interface form a linear eigenvalue problem. When inertia is neglected (Stokes flow) the problem can be determined analytically, and a dispersion equation is obtained. Such relation is solved numerically so as to study the influences of relevant parameters on the stability behavior of the flow via some diagrams.

In the general case of Orr-Sommerfeld equations, in which the effect of the Reynolds number on the stability of the two layers is considered. There are no general analytical solutions available for these equations, in which it has variable coefficients. Therefore, we discussed the case of wave motion when the wave length is very large, and then we assume that the wave number tends to zero. We depend on the viscosity ratio, the basic velocity shear, the Marangoni number that measures the effects of surfactant, electric Weber number and the capillary number measures the ratio of viscous to capillary forces. An extensive investigation is carried out that examines the stabilizing or destabilizing effects of these parameters on the flow within the two films.

Having obtained the results of the numerical applications, it is concluded that, in the case of Stokes flow depending on the selected parameters, it may be expected that a more careful search would clarify that the motion of the interfacial waves will be more stable with the increasing values of the Marangoni number, while the opposite effect is found for the increase capillary number which destabilizes the system. The dielectric constants ratio plays a destabilizing influence in the stability behavior, whereas the phenomenon of the dual role is observed increasing electric Weber number as well as viscosity ratio. In the long wave limit, the stability process is found to confirm the stabilizing effect of the Marangoni number and the destabilizing influence of both capillary and Reynolds numbers, whereas the dual role is observed for increase of the upper to lower dielectric constant ratio.

REFERENCES

Alkharashi, S. A. and Y. Gamiel (2017). Stability characteristics of periodic streaming fluids in porous media. *Theoretical and Mathematical Physics* 191(1), 580-601.

Allias, R., M. A. S. Nasir and S. A. Kechi (2017). Steady thermosolutocapillary instability in fluid layer with nondeformable free surface in the presence of insoluble surfactant and gravity. *Appl. Math. Inf. Sci.* 11(1), 87-94.

André, M. A. and M. P. Bardet (2015). Experimental study of shear layer instability below a free surface. *Physics of Fluids* 27, 112103.

Blyth, M. G. (2008). Effect of an electric field on the stability of contaminated film flow down an inclined plane. *J. Fluid Mech.* 595, 221-237.

Blyth, M. G. and C. Pozrikidis (2004). Effect of surfactants on the stability of two-layer channel flow. *J. Fluid Mech.* 505, 59-86.

Gao, P. and X. Lu (2007). Effect of surfactants on the inertialess instability of a two-layer film flow. *J. Fluid Mech.* 591, 495-507.

Halpern, D. and A. L. Frenkel (2003). Destabilization of a creeping flow by interfacial surfactant: linear theory extended to all wavenumbers. *J. Fluid Mech.* 485, 191-220.

Hayat, T., M. Imtiaz and A. Alsaedi (2016). Boundary layer flow of Oldroyd-B fluid by exponentially stretching sheet. *Applied Mathematics and Mechanics* 37(5), 573-582.

Liu, Z., G. Brenn and F. Durst (1998). Linear analysis of the instability of two-dimensional non-Newtonian liquid sheets. *J. Non-Newtonian Fluid Mech.* 78, 133-166.

Luo, H. and C. Pozrikidis (2007). Gravity-driven film flow down an inclined wall with three-dimensional corrugations. *Acta Mechanica* 188, 209-225.

Mikishev, A. B. and A. A. Nepomnyashchy (2010). Long-Wavelength Marangoni Convection in a Liquid Layer with Insoluble Surfactant: Linear Theory. *Microgravity Sci. Technol.* 22, 415-423.

Mikishev, A. B. and A. A. Nepomnyashchy (2011). Large-scale Marangoni convection in a liquid layer with insoluble surfactant under heat flux modulation. *Journal of Adhesion Science and Technology* 25, 1411-1423.

Ozen, O., N. Aubry, D. T. Papageorgiou and P. G. Petropoulos (2006). Electrohydrodynamic linear stability of two immiscible fluids in channel flow. *Electrochimica Acta* 51, 5316-5323.

Park, J. M., M. A. Hulsen and P. D. Anderson (2013). Numerical investigation of the effect of insoluble surfactant on drop formation in microfluidic device. *Eur. Phys. J. Special Topics* 222, 199-210.

Pozrikidis, C. (2003). Effect of surfactants on film flow down a periodic wall. *J. Fluid Mech*. 496, 105-127.

Shankar, V. and A. Sharma (2004). Instability of the interface between thin fluid films subjected to electric fields. *J. of Colloid and Interface Science* 274, 294-308.

Shankar, V. and L. Kumar (2004). Stability of two-layer Newtonian plane Couette flow past a deformable solid layer. *Phys. Fluids* 16 (12), 4426-4442.

Sirwah, M. A. (2012). Linear instability of the electrified free interface between two cylindrical shells of viscoelastic fluids through porous media. *Acta Mechanica Sinica* 28(6), 1572-1589.

Tomar, G., V. Shankar, A. Sharma and G. Biswas (2007). Electrohydrodynamic instability of a confined viscoelastic liquid film. *J. Non-Newtonian Fluid Mech.* 143, 120-130.

Uma, B. and R. Usha (2012). Contaminated electrified thin film over a substrate: dynamics and stability. *Int. J. Adv. Eng. Sci. Appl. Math.* 4(4), 241-249.

Wu, L. and S. Y. Chou (2005). Electrohydrodynamic instability of a thin film of viscoelastic polymer underneath a lithographically manufactured mask. *J. Non-Newtonian Fluid Mech*. 125, 91-99.

Yiantsios, S. G. and B. G. Higgins (2010). A mechanism of Marangoni instability in evaporating thin liquid films due to soluble surfactant. *Physics of* Fluids 22, 022102.

Zakaria, K. and S. A. Alkharashi (2017). Modeling and analysis of two electrified films flow traveling down between inclined permeable parallel substrates. *Acta Mech* 228, 2555-2581.

Zakaria, K., M. A. Sirwah and S. Alkharashi (2009). Instability through porous media of three layers superposed conducting fluids. *Eur. J. of Mech. B/Fluids* 28, 259-270.